J|A|C|S ARTICLES

Published on Web 09/25/2009

Insight into CH_4 Formation in Iron-Catalyzed Fischer−Tropsch Synthesis

Chun-Fang Huo,[†] Yong-Wang Li,[†] Jianguo Wang,[†] and Haijun Jiao*[,†,‡]

State Key Laboratory of Coal Conversion, Institute of Coal Chemistry, Chinese Academy of Sciences, Taiyuan 030001, People's Republic of China, and Leibniz-Institut für Katalyse e.V. an der Universität Rostock, Albert-Einstein-Strasse 29a, 18059 Rostock, Germany

Received March 19, 2009; E-mail: haijun.jiao@catalysis.de

Abstract: Spin-polarized density functional theory calculations have been performed to investigate the carbon pathways and hydrogenation mechanism for CH_4 formation on $Fe_2C(011)$, $Fe_5C_2(010)$, $Fe_3C(001)$, and $Fe_4C(100)$. We find that the surface C atom occupied sites are more active toward CH_4 formation. In Fischer−Tropsch synthesis (FTS), CO direct dissociation is very difficult on perfect Fe_xC_y surfaces, while surface C atom hydrogenation could occur easily. With the formation of vacancy sites by C atoms escaping from the Fe_xC_y surface, the CO dissociation barrier decreases largely. As a consequence, the active carburized surface is maintained. Based on the calculated reaction energies and effective barriers, CH_4 formation is more favorable on $Fe_5C_2(010)$ and $Fe_2C(011)$, while $Fe_4C(100)$ and $Fe_3C(001)$ are inactive toward CH_4 formation. More importantly, it is revealed that the reaction energy and effective barrier of CH_4 formation have a linear relationship with the charge of the surface C atom and the d-band center of the surface, respectively. On the basis of these correlations, one can predict the reactivity of all active surfaces by analyzing their surface properties and further give guides for catalyst design in FTS.

1. Introduction

Under the background of resource depletion and the unpredictable price of crude oil, utilizing coal, natural gas, and biomass to produce clean transport fuels and chemicals is attracting more and more attention.[1−5] Fischer−Tropsch synthesis (FTS), as a key technology in these processes, can convert syngas (CO/H_2) into a wide product range from methane, ethane, to high molecular hydrocarbons (mainly *n*-alkanes and *n*-alkenes) and oxygenates (Scheme 1).[6] Because CH_4 formation in FTS as byproduct wastes materials and energy, methods lowering CH_4 selectivity and raising C_{5+} selectivity are highly desired for optimizing FTS catalysts.

Because of their low price and high activity, iron-based catalysts have great perspective in energy society, but a problem that has puzzled scientists is how to suppress CH_4 formation practically. It is well-known that an iron-based catalyst is FTS active, only after reducing the precursor to a mixture of iron carbides, oxides, and metallic iron.[7−9] Although some evidences suggested iron carbides as the active phases on FTS,[7] the reaction mechanism is still unclear. To obtain a reasonable performance on reactivity, selectivity, and stability, many efforts have been made to change the reduction and carburization of the catalysts by adding promoters or adjusting pretreatment conditions.[2,9−16] For example, adding Mo to the activated-carbon supported Fe−Cu−K catalyst enhances the stability of the catalyst, but results in a higher selectivity toward CH_4 and light hydrocarbons.[10] Mg, La, and Ca promoters enhance the surface basicity of the $Fe-Cu/SiO_2$ catalyst, help the reduction and carburization, improve the FTS activity, reduce CH_4 formation,

Scheme 1. Potential Technologies for Energy Society

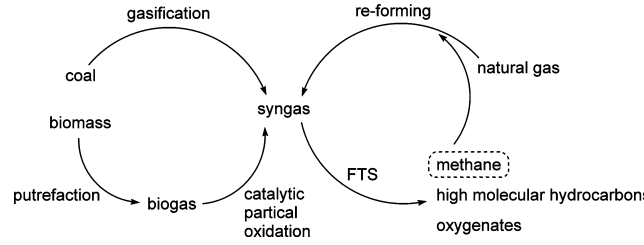

[†] Chinese Academy of Sciences.
[‡] Universität Rostock.

(1) Dry, M. E. *Appl. Catal., A* **2004**, *276*, 1, and references cited therein.
(2) Lohitharn, N.; Goodwin, J. G., Jr.; Lotero, E. *J. Catal.* **2008**, *255*, 104.
(3) Inderwildi, O. R.; Jenkins, S. J.; King, D. A. *Angew. Chem., Int. Ed.* **2008**, *47*, 5253.
(4) Liu, Z.-P.; Hu, P. *J. Am. Chem. Soc.* **2002**, *124*, 11568, and references cited therein.
(5) Inderwildi, O. R.; Jenkins, S. J. *Chem. Soc. Rev.* **2008**, *37*, 2274.
(6) Anderson, R. B. *The Fischer−Tropsch Synthesis*; Academic Press: Orlando, FL, 1984.
(7) Li, S.; O'Brien, R. J.; Meitzner, G. D.; Hamdeh, H.; Davis, B. H.; Iglesia, E. *Appl. Catal., A* **2001**, *219*, 215.
(8) Davis, B. H. *Catal. Today* **2009**, *141*, 25.
(9) Herranz, T.; Rojas, S.; Pérez-Alonso, F. J.; Ojeda, M.; Terreros, P.; Fierro, J. L. G. *J. Catal.* **2006**, *243*, 199.
(10) Ma, W.; Kugler, E. L.; Wright, J.; Dadyburjor, D. B. *Energy Fuels* **2006**, *20*, 2299.
(11) Pour, A. N.; Shahri, S. M. K.; Bozorgzadeh, H. R.; Zamani, Y.; Tavasoli, A.; Marvast, M. A. *Appl. Catal., A* **2008**, *348*, 201.
(12) Li, S.; Krishnamoorthy, S.; Iglesia, E. *Catal. Lett.* **2001**, *77*, 197.
(13) Lohitharn, N.; Goodwin, J. G., Jr. *J. Catal.* **2008**, *257*, 142.
(14) Li, S.; Krishnamoorthy, S.; Li, A.; Meitzner, G. D.; Iglesia, E. *J. Catal.* **2002**, *77*, 202.
(15) Li, T.; Yang, Y.; Zhang, C.; An, X.; Wan, H.; Tao, Z.; Xiang, H.; Li, Y.-W.; Yi, F.; Xu, B. *Fuel* **2007**, *86*, 921.
(16) Bengoa, J. F.; Alvarez, A. M.; Cagnoli, M. V.; Gallegos, N. G.; Marchetti, S. G. *Appl. Catal., A* **2007**, *325*, 68.

and increase the selectivity of high molecular hydrocarbons.[11] Bengoa et al. showed that the Fe/C catalysts having an intermediate reduction species in the fresh reduced state, Fe_3O_4(sp), produce a nonstoichiometric iron carbide, which exhibits a higher FTS activity and light olefins selectivity.[16] These suggest that the reactivity of a catalyst is correlated with the properties of iron carbides. Therefore, maintaining a carburized surface or forming active carbides is the main issue for catalysis design.

In 1988, the carbon pathway for methanation and chain growth during FTS on Fe/Al_2O_3 catalyst was studied by switching $^{12}CO/H_2$ to $^{13}CO/H_2$. It was found that several hydrogen-free monolayer carbons are present on the Fe surface and can exchange with ^{13}C in the rate of about 3% of the overall synthesis.[17] Using in situ Mössbauer spectroscopy and temperature-programmed hydrogenation (TPH), Xu and Bartholomew characterized carbonaceous surface species and bulk iron carbides formed during FTS reaction on silica-supported iron-catalysts.[18] They divided carbon species into four types, (a) C_α (atomic carbon, adsorbed or surface carbides), (b) C_β (amorphous, lightly polymerized hydrocarbon or carbon surface species), (c) C_γ (bulk iron carbides, ε' $Fe_{2.2}C$ and χ Fe_5C_2), and (d) C_δ (disordered and moderately ordered graphitic surface carbons), and found that the initial catalytic activity is positively correlated with the amount of reactive C_α formed on the catalyst surface. Recently, the methanation reaction mechanism under FTS conditions was investigated with the steady-state isotopic transient kinetic analysis (SSITKA) technique over a precipitated iron-based catalyst.[19] The results showed that there are two active carbon pools (C_α and C_β) on the catalyst surface, and the C_β pool is 25−50 times less active than the C_α pool for methanation, while the C−C coupling reaction involves both the C_α and the C_β pools. Nevertheless, the relationships between the microstructure and properties of iron carbides and the reactivity of CH_4 formation cannot be established on the basis of the available experimental evidences.

In this work, we have performed a detailed DFT study on the mechanisms of CH_4 formation on the Fe_2C, Fe_5C_2, Fe_3C, and Fe_4C surfaces. First, we are interested in the carbon pathways for CH_4 formation. Next, the mechanisms of carbon hydrogenation to CH_4 are discussed. Finally, the correlations between the surface properties of iron carbides and the reactivity for CH_4 formation are established, and a deep insight into these relationships is proposed.

2. Computational Details

2.1. Methods. All calculations were performed at the density functional theory (DFT) level within the Vienna Ab initio Simulation Package (VASP/Version 4.6).[20] The exchange and correlation energies were calculated using the Perdew, Burke, and Ernzerhof (PBE) functional.[21] The electron−ion interaction was described by the projector augmented wave (PAW) method,[22] and the Kohn−Sham one-electron states were expanded in a plane wave basis set up to 400 eV. Because of its large effect on the adsorption energies for magnetic systems,[23−25] spin-polarization was included. For evaluating the energy barriers, all transition states were located using the Nudged Elastic Band (NEB) method.[26] Furthermore, the vibrational frequencies were analyzed to evaluate if a stationary point is a minimum state without imaginary frequencies or a transition state with only one imaginary frequency.

Based on the DFT calculated results, adsorption energy, reaction energy, and barrier are used to describe the thermodynamic and kinetic properties of the reactions. The adsorption energy is defined as $E_{ads} = E(\text{adsorbates/slab}) - [E(\text{slab}) + E(\text{adsorbates})]$, where E(adsorbates/slab) is the total energy of the slab with adsorbates, E(slab) is the total energy of the corresponding bare Fe_xC_y slab, and E(adsorbates) is the total energy of free adsorbates. Therefore, the more negative the E_{ads}, the stronger the adsorption. The reaction energy and barrier are calculated by $\Delta_r E = E(\text{FS}) - E(\text{IS})$ and $E_a = E(\text{TS}) - E(\text{IS})$, where E(IS), E(FS), and E(TS) are the energies of the corresponding initial state (IS), final state (FS), and transition state (TS), respectively. In all calculated energy data, the zero-point energy (ZPE) has been taken into account.

2.2. Models. Because the unit cell of the Fe_2C, Fe_5C_2, Fe_3C, and Fe_4C crystals is orthorhombic, monoclinic, orthorhombic, and cubic, respectively, the most stable surfaces of $Fe_2C(011)$,[27] $Fe_5C_2(010)$,[28] $Fe_3C(001)$,[29] and $Fe_4C(100)$[30] were chosen as the samples for direct comparison. In this work, the periodic slab models were employed. For modeling the $Fe_2C(011)$, $Fe_5C_2(010)$, and $Fe_3C(001)$ surfaces, the slabs consisting of five-layer iron and three-layer carbon, four-layer iron and four-layer carbon, as well as four-layer iron and four-layer carbon are used, respectively. In all calculations, the top three-layer iron and one-layer carbon, two-layer iron and two-layer carbon, as well as two-layer iron and three-layer carbon were allowed to relax, while the corresponding bottom layers were fixed in their bulk positions. For $Fe_4C(100)$, a four-layer model was used, and the top two-layer was allowed to relax, while the bottom two-layer was fixed. Without counting the adsorbates, the vacuum between the slabs was set to span a range of 10 Å to exclude slab interactions. The top and side views of the studied Fe_xC_y surfaces are illustrated in Figure 1.

To minimize the coverage effect for the direct comparison, different unit cells, $p(1 \times 1)$ for $Fe_2C(011)$, $Fe_5C_2(010)$, $Fe_3C(001)$ and $p(\sqrt{2} \times \sqrt{2})$ for $Fe_4C(100)$, were chosen to make the surface unit cell lattice vectors as close as possible. According to lattice size, a $5 \times 5 \times 1$ k grid sampling within the Brillouin zones was set, except it was $3 \times 5 \times 1$ for $Fe_5C_2(010)$. From Table 1, we can see that the $p(1 \times 1)$ $Fe_2C(011)$ has the smallest lattice size. Therefore, reaction energy and barrier for the $CH + 3H \rightarrow CH_2 + 2H$ step were examined on $Fe_2C(011)$ using a $p(2 \times 1)$ unit cell. This increase of unit cell size results in the energy changes by less than 0.05 eV. This indicates that the calculated results on a series of Fe_xC_y surfaces are reasonable and comparable.

(17) Stockwell, D. M.; Bianchi, D.; Bennett, C. O. *J. Catal.* **1988**, *113*, 13.
(18) Xu, J.; Bartholomew, C. H. *J. Phys. Chem. B* **2005**, *109*, 2392.
(19) Govender, N. S.; Botes, F. G.; de Croon, M. H. J. M.; Schouten, J. C. *J. Catal.* **2008**, *260*, 254.
(20) (a) Kresse, G.; Hafner, J. *Phys. Rev. B* **1993**, *48*, 13115. (b) Kresse, G.; Furthmüller, J. *Comput. Mater. Sci.* **1996**, *6*, 15. (c) Kresse, G.; Furthmüller, J. *Phys. Rev. B* **1996**, *54*, 11169.
(21) Perdew, J. P.; Burke, K.; Ernzerhof, M. *Phys. Rev. Lett.* **1996**, *77*, 3865.
(22) Blöchl, P. E. *Phys. Rev. B* **1994**, *50*, 17953.
(23) Nayak, S. K.; Nooijen, M.; Bernasek, S. L. *J. Phys. Chem. B* **2001**, *105*, 164.
(24) Cheng, H. S.; Reiser, D. B.; Dean, S. W., Jr.; Baumert, K. *J. Phys. Chem. B* **2001**, *105*, 12547.
(25) Ge, Q.; Jenkins, S. J.; King, D. A. *Chem. Phys. Lett.* **2000**, *327*, 125.
(26) Jónsson, H.; Mills, G.; Jacobsen, K. W. *Classical Quantum Dynamics in Condensed Phase Simulations*; World Scientific: Singapore, 1998; p 385.
(27) Bao, L.-L.; Huo, C.-F.; Deng, C.-M.; Li, Y.-W. *J. Fuel Chem. Technol.* **2009**, *37*, 104.
(28) Steynberg, P. J.; van den Berg, J. A.; van Rensburg, W. J. *J. Phys.: Condens. Matter* **2008**, *20*, 064238.
(29) (a) Chiou, W. C., Jr.; Carter, E. A. *Surf. Sci.* **2003**, *530*, 87. (b) Liao, X.-Y.; Cao, D.-B.; Wang, S.-G.; Ma, Z.-Y.; Li, Y.-W.; Wang, J. G.; Jiao, H. *J. Mol. Catal. A* **2007**, *269*, 169. (c) Liao, X.-Y.; Wang, S.-G.; Ma, Z.-Y.; Li, Y.-W.; Wang, J.; Jiao, H. *J. Mol. Catal. A* **2008**, *292*, 14.
(30) Deng, C.-M.; Huo, C.-F.; Bao, L.-L.; Shi, X.-R.; Li, Y.-W.; Wang, J.; Jiao, H. *Chem. Phys. Lett.* **2007**, *448*, 83.

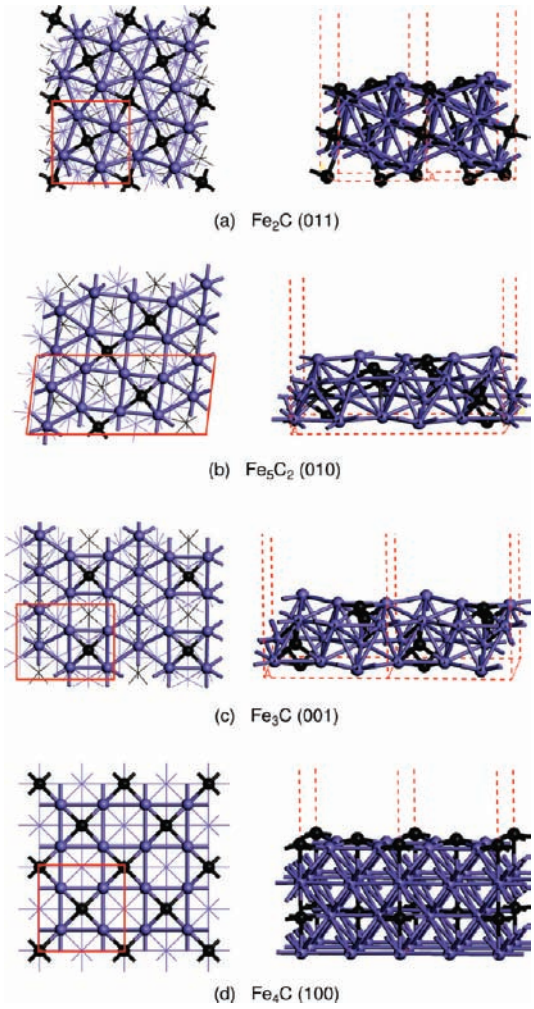

Figure 1. Top and side views of the Fe_xC_y surfaces (blue, Fe atom; black, C atom) (frame in top views shows the unit cell used in calculations: $p(1 \times 1)$ for $Fe_2C(011)$, $Fe_5C_2(010)$, $Fe_3C(001)$ and $p(\sqrt{2} \times \sqrt{2})$ for $Fe_4C(100)$).

Table 1. Structure Parameters of the Selected Fe_xC_y Models[a]

	$Fe_2C(011)$	$Fe_5C_2(010)$	$Fe_3C(001)$	$Fe_4C(100)$
u/Å	4.651	5.060	5.090	5.289
v/Å	5.099	11.562	6.740	5.289
total layers	5Fe/3C	4Fe/4C	4Fe/4C	4
relaxed layers	3Fe/1C	2Fe/2C	2Fe/3C	2

[a] (u, v) are the surface unit cell lattice vectors.

3. Results and Discussion

3.1. Structure of the Iron Catalysts. To obtain the FTS activity, the iron oxide precursor must be pretreated in CO, H_2, or syngas (CO/H_2). During the activation process, iron oxide first transforms from α-Fe_2O_3 to Fe_3O_4 irrespective of the activation gas used for pretreatment. After that, the nature of the iron phases depends on the activating atmosphere. Under CO or CO/H_2 atmosphere, iron carbides are formed at the exterior of Fe_3O_4 crystallites, leading to a surrounding core structure. Hydrogen activation of iron-based samples yields metallic iron, which evolves into iron carbide species under the FTS environment.[7−9,18] Experimental evidences showed that an active iron catalyst has a dynamic pseudosteady-state during FTS with a slow continuous replacement of carbon in the iron carbide layers.[8] Therefore, maintaining the structure and thickness of the iron carbide layers under the reaction conditions determines the stability of the catalyst.

3.2. Carbon Pathways for CH_4 Formation. Because the carbon atoms of the iron carbides come from CO and can take part in FT reactions, exploring the carbon pathways for CH_4 formation is very interesting to the iron-catalyzed FTS. When exposing the iron carbides to syngas, two kinds of reactions may occur at first. One is the dissociation or hydrogenation of the adsorbed CO; and the other is the surface C atom hydrogenation or coupling with CO. Here, all possible reactions are considered on the $Fe_2C(011)$, $Fe_5C_2(010)$, $Fe_3C(001)$, and $Fe_4C(100)$ surfaces. The optimized structures and the related reaction energies are given in Figures 2 and 3.

As shown in Figure 2, CO adsorbs at the Fe-top or 4-fold site uprightly on $Fe_2C(011)$, $Fe_3C(001)$, and $Fe_4C(100)$. Because all first layer Fe atoms of $Fe_2C(011)$ and $Fe_4C(100)$ bind with C atoms, CO dissociation on these surfaces will lead to $C_{(s)}-C$ and O species, in which $C_{(s)}-C$ occupies the 4-fold site through both C atoms, and O resides at the 3-fold or 4-fold site. This process is highly endothermic by 2.79 or 2.24 eV and thus cannot occur directly under FTS conditions. Surface C hydrogenation is potentially competitive to CO hydrogenation. On $Fe_2C(011)$ and $Fe_4C(100)$, 3-fold or 4-fold adsorbed H atom migrates to CO, resulting in the Fe-top adsorbed CHO species. It is predicted to be endothermic by 0.93 and 1.32 eV, with barriers of 0.95 and 1.36 eV, respectively. In comparison, surface C hydrogenation to CH has the lower endothermic character (0.37 and 0.54 eV) and barriers (0.40 and 0.74 eV) and thus is more favored thermodynamically and kinetically. An alternative path is CO coupling with surface C atom forming the uprightly adsorbed $C_{(s)}CO$ species. It is computed to be endothermic by 0.87 and 0.62 eV and to have moderate barriers of 0.93 and 0.64 eV, respectively. These indicate that $C_{(s)}CO$ is likely one of the instantaneous intermediates in chain growth on $Fe_2C(011)$ and $Fe_4C(100)$.

Similar to that on $Fe_2C(011)$ and $Fe_4C(100)$, surface C hydrogenation to CH on $Fe_3C(001)$ is more competitive than CO hydrogenation to CHO both kinetically and thermodynamically. As shown in Figure 2, CHO interacts with the $Fe_3C(001)$ surface by C and O atoms occupying the adjacent Fe top site. Although CO dissociation on $Fe_3C(001)$ leads to the 3-fold adsorbed C and O atoms, it cannot occur yet due to the high barrier of 1.69 eV. On the other hand, the $C_{(s)}-CO$ coupling reaction is hindered kinetically (1.89 eV) on $Fe_3C(001)$.

As shown in Figure 1, the $Fe_5C_2(010)$ surface presents a complex pattern of Fe and C atoms. The middle region has both Fe and C atoms, while the left and right regions have only Fe atoms in the top layer. Sorescu's study revealed that CO prefers adsorption on the Fe-only region. In the C−O most activated configuration, CO adsorbs on the surface in the lying-down model by forming three Fe−C and two Fe−O bonds (Figure 3). Taking this configuration as a starting point, CO dissociation to the 4-fold adsorbed C and 3-fold adsorbed O atoms is nearly thermoneutral (−0.05 eV), but still has a high barrier of 1.43 eV. In comparison, hydrogenation reactions can occur more easily. Under low H_2 partial pressure, CO and H coadsorb in model A with H adatom at the 3-fold site of CO's O side. In this case, CO hydrogenation will lead to COH species adsorbed at the 4-fold site via C atom. From Figure 3, we can see that surface C hydrogenation to CH is preferred both thermodynamically (0.31 eV) and kinetically (0.92 eV), while CO hydrogenation to COH is hindered by the high barrier of 1.77 eV. As H_2 partial pressure increases, the dissociative H atom occupying

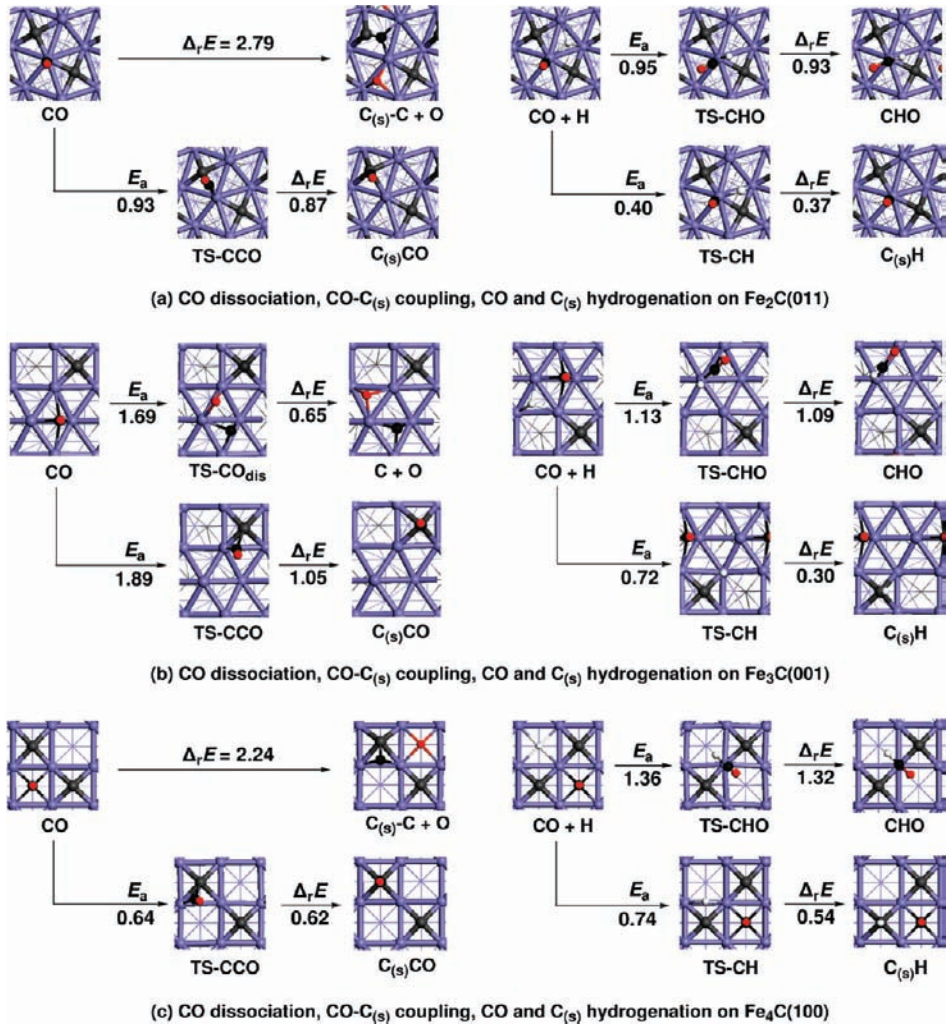

Figure 2. Structures of key stationary points and reaction energies/barriers ($\Delta_r E$ and E_a, eV) for reactions involved in the carbon pathways on $Fe_2C(011)$, $Fe_3C(001)$, and $Fe_4C(100)$ (blue, Fe atom; black, C atom; red, O atom; white, H atom).

the bridge site of CO's C side in model B becomes possible. In this case, CO hydrogenation to the lying-down CHO is competitive with surface C hydrogenation to CH, as indicated by their close barriers (0.16 vs 0.23 eV). As compared to CO direct dissociation, CHO dissociation to CH and O species is much easier with a lower barrier of 0.45 eV and is exothermic by −0.82 eV. It is also to note that rising from the very high barrier of 2.04 eV, the $C_{(s)}$−CO coupling reaction cannot occur on $Fe_5C_2(010)$.

On the basis of the above discussion, we can conclude that surface C hydrogenation is a very important reaction in every case. With a surface C atom escaping from the Fe_xC_y surface via methanation or producing hydrocarbon, a vacancy site (v) will emerge on the Fe_xC_y surface. Whether this vacancy site can be filled in time is the key point for maintaining the catalyst stability. For answering this question, CO adsorption and dissociation on the vacancy site have been examined. The optimized structures are illustrated in Figure 4, while the compared energy data on the perfect and vacancy surfaces are summarized in Table 2. As expected, CO adsorption on the vacancy site has a larger adsorption energy (−2.07 vs −1.32 eV, −1.90 vs −1.77 eV, −1.92 vs −1.83 eV, and −2.20 vs −1.14 eV, respectively) and lower dissociation barrier (0.84 vs >2.79 eV, 1.07 vs 1.43 eV, 0.91 vs 1.69 eV, and 0.93 vs >2.24 eV, respectively) than those on the perfect $Fe_2C(011)$, $Fe_5C_2(010)$, $Fe_3C(001)$, and $Fe_4C(100)$ surfaces. Therefore, once the vacancy site is formed, CO will adsorb and dissociate on this site prior to other sites, and thus refresh the catalyst.

At this time, the main carbon pathways for CH_4 formation on the Fe_xC_y surfaces can be outlined as follows, and our ongoing investigation on the mechanism of CH_4 formation is focused on surface C hydrogenation.

$$C_{(s)} + H_{(ads)} \rightarrow CH_{(ads)}$$

$$CH_{(ads)} + H_{(ads)} \rightarrow CH_{2(ads)}$$

$$CH_{2(ads)} + H_{(ads)} \rightarrow CH_{3(ads)}$$

$$CH_{3(ads)} + H_{(ads)} \rightarrow CH_{4(g)}$$

$$v + CO_{(g)} \rightarrow CO_{(ads)}$$

$$CO_{(ads)} \rightarrow C_{(s)} + O_{(ads)}$$

3.3. Mechanism for Carbon Hydrogenation to CH_4. As the initial state for methanation, two H_2 molecules were put to 1.750 Å above the surface Fe atom (from the low energy electronic

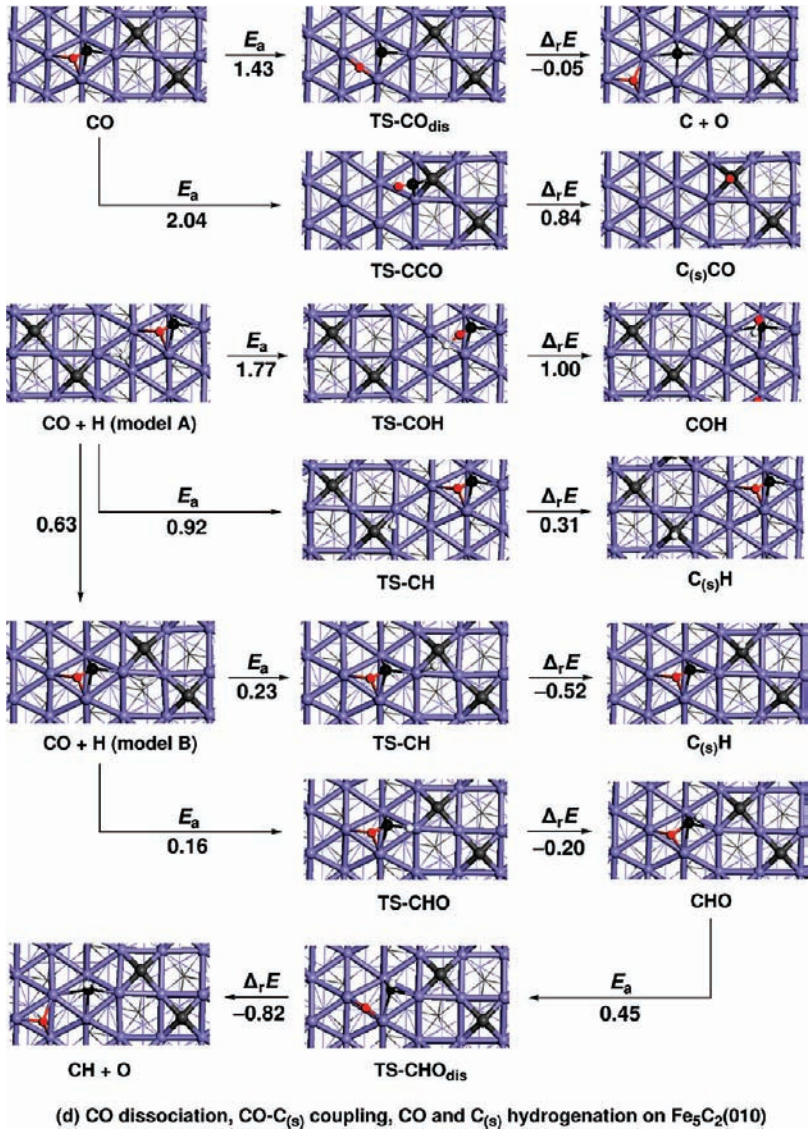

Figure 3. Structures of key stationary points and reaction energies/barriers ($\Delta_r E$ and E_a, eV) for reactions involved in the carbon pathways on $Fe_5C_2(010)$ (blue, Fe atom; black, C atom; red, O atom; white, H atom).

diffraction experiment[31]) or 1.250 Å above the surface C atom (based on the bond length of C−H) with the H−H distance of 0.753 Å. The results show that hydrogen prefers adsorption on the Fe atoms in molecular and dissociative states. Neither molecular adsorption nor directly dissociative adsorption can be found on the surface C atom. Taking these adsorption models as starting points for studying carbon hydrogenation, all intermediates and transition states were located on the $Fe_2C(011)$, $Fe_5C_2(010)$, $Fe_3C(001)$, and $Fe_4C(100)$ surfaces along the reaction path coordinate and are displayed in Figure 5. Following the successive hydrogenation steps, the corresponding intermediates $(H_2 + 2H)/(4H)$, $(H_2 + H + CH)/(3H + CH)$, $(H_2 + CH_2)/(2H + CH_2)$, $(H + CH_3)$, and CH_4 are notated as **1a/1b**, **2a/2b**, **3a/3b**, **4**, and **5**, respectively. For mapping the reaction energy profiles of $Fe_xC_y + 2H_2 \rightarrow Fe_xC_{(y-1)} + CH_4$, the sum of the total energies of the bare Fe_xC_y slab and two free H_2 molecules was taken as the origin. Hence, the relative energy of each species in Figure 6 can be expressed as $E(2H_2)_{ads} = E(\text{adsorbates/slab}) - [E(\text{slab}) + 2E(H_2)]$.

On $Fe_2C(011)$, $Fe_5C_2(010)$, $Fe_3C(001)$, and $Fe_4C(100)$, the surface carbon atoms coordinate with four iron atoms in different steric structure and arrangement (Figure 1). Exposed to syngas, these surface carbon atoms can react with H atoms to form surface CH_x ($x = 1-3$) species, and then take part in chain growth or further hydrogenate to CH_4. For CH and CH_2 species, the C atom resides at the 4-fold site but slightly moves up on all Fe_xC_y surfaces. The C−H bond of CH species is nearly perpendicular to the four-iron consisted plane, while one C−H bond of the CH_2 species interacts agostically with one or two surface iron atoms. For CH_3 species, the C atom shifts to the bridge site in all cases. Unlike surface CH_x ($x = 1-3$), CH_4 is only weakly physisorbed. As the experimental observation on TiC(111), ZrC(111), HfC(111), and NbC(111),[32] all Fe_xC_y surfaces can dissociate hydrogen easily with low barriers of less than 0.16 eV (**2−2a → 2−2b**, **2.5−1a → 2.5−1b**, and **4−3a → 4−3b**, Figure 6). The dissociative H atoms normally occupy the 3-fold or 4-fold site in the stable configurations and migrate to the top or bridge site in the transition states for hydrogenation.

(31) Moritz, W.; Imbihl, R.; Behm, R. J.; Ertl, G.; Matsushima, T. *J. Chem. Phys.* **1985**, *83*, 1959.

(32) Aizawa, T.; Hayami, W.; Souda, R.; Otani, S.; Ishizawa, Y. *Surf. Sci.* **1997**, *381*, 157.

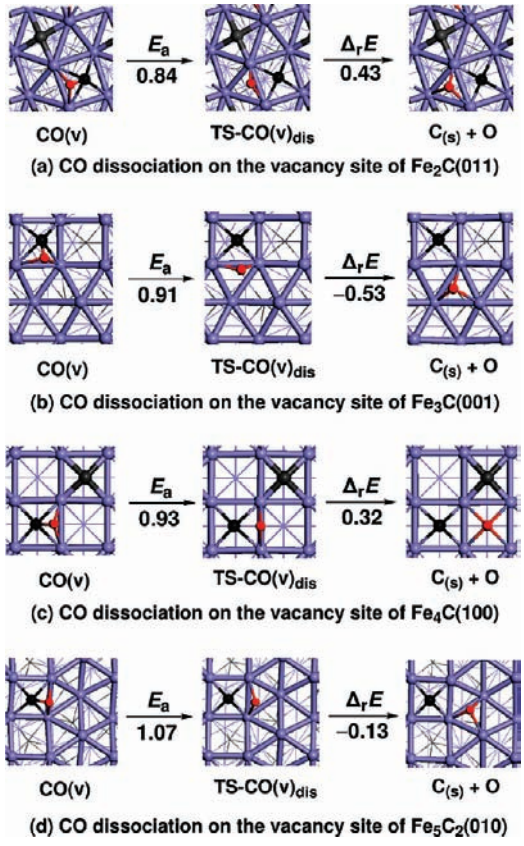

Figure 4. Structures of key stationary points and reaction energies/barriers ($\Delta_r E$ and E_a, eV) for CO dissociation on the vacancy site of $Fe_2C(011)$, $Fe_3C(001)$, $Fe_4C(100)$, and $Fe_5C_2(010)$ (blue, Fe atom; black, C atom; red, O atom).

Table 2. Energy Data for CO Adsorption and Dissociation on the Fe_xC_y Surfaces

		$E(CO)_{ads}$/eV	E_a/eV	$\Delta_r E$/eV
$Fe_2C(011)$	perfect	−1.32		2.79
	vacancy	−2.07	0.84	0.43
$Fe_5C_2(010)$	perfect	−1.77	1.43	−0.05
	vacancy	−1.90	1.07	−0.13
$Fe_3C(001)$	perfect	−1.83	1.69	0.65
	vacancy	−1.92	0.91	−0.53
$Fe_4C(100)$	perfect	−1.14		2.24
	vacancy	−2.20	0.93	0.32

Despite the high structural similarity of surface CH_x and close ability to dissociate hydrogen, the Fe_xC_y surfaces exhibit different kinetic and thermodynamic characteristics for CH_4 formation.

On $Fe_2C(011)$, C and CH_3 are the most stable C_1 species. As shown in Figure 6, both C + H → CH (**2−1a → 2−2a**) and CH + H → CH_2 (**2−2b → 2−3b**) are endothermic processes (0.39 and 0.49 eV) with barriers of 0.40 and 0.49 eV, respectively. However, CH_2 + H → CH_3 (**2−3b → 2−4**) is highly exothermic by −1.09 eV and has a barrier of 0.33 eV. Because the reverse reactions of C + H → CH and CH + H → CH_2 have nearly no barriers, the dehydrogenation reactions of CH and CH_2 occur easily. It is to note that the typical reaction temperatures are 473−513 K for the low-temperature FTS process and 573−623 K for the high-temperature FTS process. Under these conditions, the apparent barrier of 1.36 eV for **2−1a → 2−4** could be overcome, leading to CH_3 species. Along the methanation coordinate, the last hydrogenation step leading to CH_4 (**2−4 → 2−5**) has the highest barrier of 1.27 eV.

Unlike $Fe_2C(011)$, CH and CH_2 are the most stable C_1 species on $Fe_5C_2(010)$. Among the sequential hydrogenation steps leading to CH_4 formation, the first C + H → CH (**2.5−1b → 2.5−2b**) and second CH + H → CH_2 (**2.5−2b → 2.5−3b**) steps can occur easily with low barriers of 0.23 and 0.12 eV, respectively. Moreover, the first hydrogenation step is predicted to be exothermic by −0.52 eV, while the second hydrogenation step is slightly endothermic by 0.10 eV. The third CH_2 + H → CH_3 (**2.5−3b → 2.5−4**) and fourth CH_3 + H → CH_4 (**2.5−4 → 2.5−5**) steps are endothermic by 0.63 and 0.33 eV with moderate barriers of 0.72 and 0.81 eV, respectively.

On $Fe_3C(001)$, hydrogen can easily cleave into the adsorbed H and CH species on the Fe−C hybrid site. The unique exothermic characteristics of −0.51 eV for C + H_2 → CH + H (**3−1a → 3−2b**) lead to CH as the most stable C_1 species. It can further hydrogenate to surface CH_2 (**3−2b → 3−3b**) by elevating 0.88 eV in energy. Noteworthy, surface CH_2 dehydrogenates to CH without any barrier, but the sequential hydrogenation steps to CH_3 (**3−3b → 3−4**) and CH_4 (**3−4 → 3−5**) need to overcome relatively high barriers of 0.89 and 0.91 eV, respectively. These indicate that the thermodynamic stability of the CH species determines the thermochemistry of the reaction.

$Fe_4C(100)$ is a very flat surface. Hydrogen dissociation from the top site to two 4-fold hollow sites (**4−3a → 4−3b**) is highly exothermic by −1.04 eV. It is to note that the dissociative H atom embeds in the first layer and has a weak interaction with the second layer Fe atom. Thus, a lower reactivity of the adsorbed H atom is expected. As shown in Figure 6, the successive hydrogenation steps, C + H → CH (**4−1a → 4−2a**), CH + H → CH_2 (**4−2a → 4−3a**), and CH_2 + H → CH_3 (**4−3b → 4−4**), are endothermic by 0.54, 0.93, and 0.51 eV, with barriers of 0.74−0.93 eV. Furthermore, the last hydrogenation step to form CH_4 (**4−4 → 4−5**) has the highest barrier of 1.00 eV and is nearly thermoneutral.

3.4. Factors Controlling CH_4 Formation on Fe_xC_y. At this stage, one may ask what are the factors controlling CH_4 formation on the Fe_xC_y surfaces. To answer this question, the properties of Fe_xC_y surfaces and the reactivity for CH_4 formation are analyzed and summarized in Table 3. $q(C_{surf})$ is the Mulliken charge of the surface C atom. ε_d is the location of the d-band center relative to the Fermi energy. As we know, the reactivity of a reaction should include both thermodynamic and kinetic aspects. Thermodynamically, the reactivity for CH_4 formation on the Fe_xC_y surfaces can be described by the reaction energy of the whole reaction. Because of the CH_4 weak physisorption in the final state (**m-5**), the reaction energy of Fe_xC_y + $2H_2$ (g) → $Fe_xC_{(y-1)}$ + CH_4 (g) can be calculated as $\Delta_r E = E(CH_4/slab) - E(slab) - 2E(H_2) = E(2H_2)_{ads}$(**m-5**). Kinetically, the effective barrier of the surface reactions has been used to describe CH_4 formation on Rh, Co, Ru, Fe, and Re surfaces in FTS successfully,[33] which is defined as the energy difference between the highest transition state (TS) and the most stable C_1 species. For $Fe_2C(011)$ and $Fe_4C(100)$, C is the most stable C_1 species, and **TS*i*** has the highest energy (i = 3 and 4, respectively). Thus, the CH_4 formation rate can be expressed as $r_{CH_4} = A\theta_C\theta_{H_2}(\theta_H/\theta_*)^{(i-2)}e^{-E_{eff}/RT}$. For $Fe_5C_2(010)$ and $Fe_3C(001)$, CH is the most stable C_1 species, so the rate equation can be described as r_{CH_4}

(33) Cheng, J.; Hu, P.; Ellis, P.; French, S.; Kelly, G.; Lok, C. M. *J. Phys. Chem. C* **2009**, *113*, 8858.

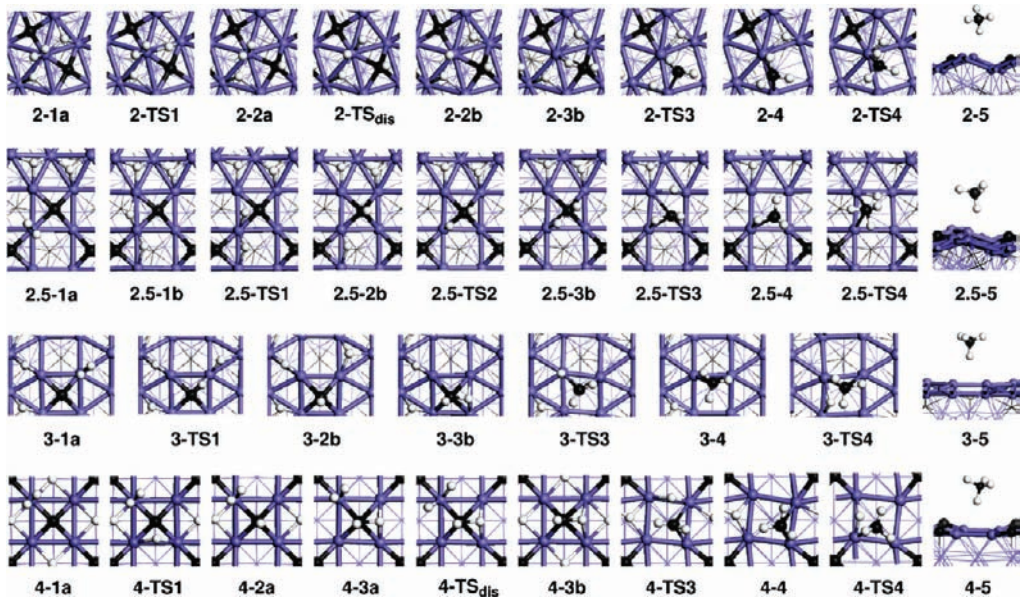

Figure 5. Structures for stationary points involved in CH_4 formation on $Fe_2C(011)$, $Fe_5C_2(010)$, $Fe_3C(001)$, and $Fe_4C(100)$ (blue, Fe atom; black, C atom; white, H atom).

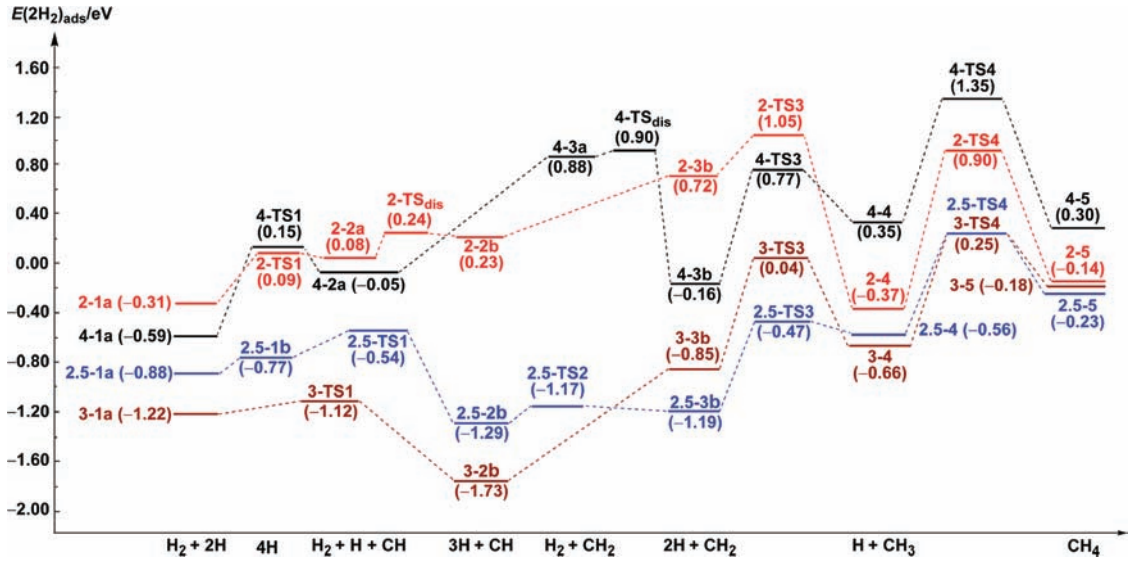

Figure 6. Energy profiles for CH_4 formation on the $Fe_2C(011)$, $Fe_5C_2(010)$, $Fe_3C(001)$, and $Fe_4C(100)$ surfaces (notation **m**−**n**: **m** = Fe/C and **n** represents species; **TS1**−**4** correspond to C + H → CH, CH + H → CH_2, CH_2 + H → CH_3, and CH_3 + H → CH_4, respectively).

Table 3. Fe_xC_y Surface Properties as well as Reaction Energies ($\Delta_r E$) and Effective Barriers (E_{eff}) for CH_4 Formation on the Fe_xC_y Surfaces

	$Fe_2C(011)$	$Fe_5C_2(010)$	$Fe_3C(001)$	$Fe_4C(100)$
Fe/C_{surf}	2	5	6	2
$q(C_{surf})^a$/e	−0.72	−0.68	−0.70	−0.76
$E(C)_{ads}$/eV	−8.62	−8.45	−8.56	−9.02
ε_d/eV	−1.42	−1.35	−1.28	−1.28
$\Delta_r E$/eV	−0.14	−0.23	−0.18	0.30
E_{eff}/eV	1.36	1.54	1.98	1.94

[a] Mulliken charge.

$= A\theta_{C\{H\}}\theta_H(\theta_H/\theta_*)^2 e^{-E_{eff}/RT}$. In these equations, A is the pre-exponential factor, E_{eff} is the effective barrier for CH_4 formation, and θ_C, θ_{CH}, θ_{H_2}, θ_H, and θ_* are the coverages of C, CH, H_2, H, and free surface site. The pre-exponential factor A is usually around 10^{13} for surface reactions (adsorption and desorption excluded).[34] $\theta_C\theta_{H_2}(\theta_H/\theta_*)^{(i-2)}$ or $\theta_{CH}\theta_H(\theta_H/\theta_*)^2$ is determined by the balance between CO activation, chain growth, and termination processes, and is strongly influenced by reaction temperature, pressure, and H_2/CO ratio. Its estimation is beyond the scope of this Article. It is noteworthy that the reaction rate changes with the effective barrier exponentially. At 500 K, an E_{eff} change of 0.1 eV will lead to a 10-fold change of r_{CH_4}. Therefore, taking the effective barrier as a descriptor to estimate the CH_4 formation rate on a series of Fe_xC_y surfaces is expected. From Table 3, we can see that reaction energy ($\Delta_r E$) and effective barrier (E_{eff}) for CH_4 formation have no direct correlation with the ratio of Fe to C, while they exhibit a linear relationship with the charge of the surface C atom ($R^2 = 0.97$ for $\Delta_r E \sim q(C_{surf})$ in Figure 7)[35] and the d-band center of the surface ($R^2 = 0.96$ for $E_{eff} \approx \varepsilon_d$ in Figure 7), respectively. On

(34) Boudart, M.; Djéga-Mariadassou, G. *Kinetics of Heterogeneous Catalytic Reactions*; Princeton University Press: Princeton, NJ, 1984.

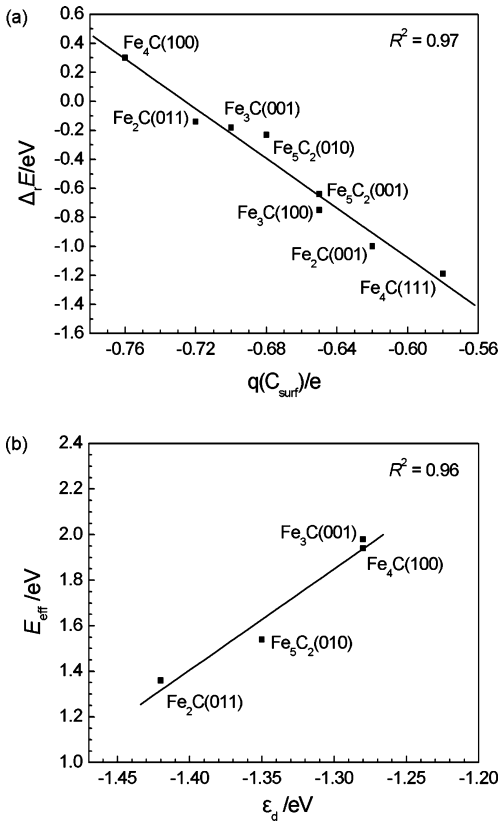

Figure 7. Relationships between reaction energy ($\Delta_r E$) of CH_4 formation and Mulliken charge (q) of the surface C atom as well as effective barrier (E_{eff}) of CH_4 formation and d-band center (ε_d) of the surface.

the basis of these correlations, we cannot only predict the reactivity for CH_4 formation on all active Fe_xC_y surfaces via analyzing their surface properties, but also can deduce that the promoters, which can increase the charge of surface carbon atoms, will decrease the CH_4 selectivity in iron-catalyzed FTS. The effect of the promoters will be our next research topic.

Now we would like to shed light on the essential parts of these linear relationships. In Fe_xC_y systems, Fe atoms are positively charged, and C atoms are negatively charged. As shown in Figure 1, surface C atoms of iron carbides can be considered as adatoms adsorbing on the defective Fe-terminated surfaces. From Table 3, we can see that the less negatively charged the surface C atom, the weaker the bonding between the corresponding C atom and the surface. It is well-known that the chemical bonding between an adsorbate and the metal surface controls the adsorbate's potential reactivity. Weaker adsorbate−surface bonds generally help enhance bonding-making processes or association reactions.[36] If the C atom binds weakly with the surface, its removal will cost less energy. Therefore, the less negative charged the surface C atom, the more exothermic (or less endothermic) the CH_4 formation reaction.

On the other hand, carbon hydrogenation to CH_4 involves the successive insertion of H atom to Fe−C bond. The mechanism is more easily analyzed by examining the reverse process. The activation of C−H is primarily guided by the electron back-donation from Fe atoms into the antibonding σ_{CH}* state of CH_x.[36] Hence, it is expected that the C−H bond activation barriers decrease as the surface d-band center shifts closer to the Fermi energy. Conversely, the surface where the d-band center is far from the Fermi energy is more active for hydrogenation and should have the lower effective barrier for CH_4 formation. This is in agreement with Pallassana and Neurock's finding on ethylene hydrogenation.[37]

3.5. Comparison of Pure Metals and Iron Carbides. On Rh(211), Fe(210), and stepped Ru, Co, and Re(001) surfaces, Hu and co-workers found that the total energies along the coordinate of C hydrogenation to CH_4 increase in a stepwise manner. This indicated that C is the most stable surface C_1 species, and CH_3 hydrogenation is the rate-determining step in sequential hydrogenation reactions.[33] However, not all pure metal surfaces obey this kind of stepwise-increasing energy profile. On Ru(1120), CH and CH_2 are found to be the most stable C_1 species, and CH_3 hydrogenation is the rate-determining step.[38] On Fe(100), CH is the most stable C_1 species, and CH_2 hydrogenation has the highest energy barrier.[39] These indicate that both geometric and electronic structures can affect the reactivity of CH_4 formation on metal surfaces. In iron carbides, insertion of C atoms into Fe lattice changes both geometric and electronic structures with respect to the parent metal. As shown in Figure 1, the surfaces of iron carbides become more corrugated in most cases. Because they have similar geometric structures, it is possible to make a direct comparison in electronic terms of $Fe_4C(100)$ and Fe(100). Insertion of C atoms leads the d-band center of the surface to shift from −1.34 to −1.28 eV. Consequently, the effective barrier for CH_4 formation increases from 1.22 eV (without ZPE) on Fe(100)[39] to 1.94 eV on $Fe_4C(100)$. Therefore, carburization of an iron catalyst is important for obtaining a desired hydrogenation activity and hydrocarbon distribution in FTS.

4. Conclusion

In this Article, the carbon pathway and hydrogenation mechanism for CH_4 formation on $Fe_2C(011)$, $Fe_5C_2(010)$, $Fe_3C(001)$, and $Fe_4C(100)$ were investigated at the density functional theory level. It is found that the surface C atom occupied sites are more active toward CH_4 formation. CO direct dissociation on the perfect Fe_xC_y surfaces is very difficult or even cannot occur rising from their very high barriers of 1.43−2.79 eV. On the other hand, surface C hydrogenation to CH is more preferred as compared to CO hydrogenation. Consequently, surface C atoms will escape from the Fe_xC_y surfaces via methanation or producing hydrocarbons. The formed vacancy sites enhance the CO adsorption by 0.09−1.06 eV, and largely lower the CO dissociation barrier to 0.84−1.07 eV. Therefore, the vacancy sites can be redeposited by CO dissociation in time, and the active carburized surface is maintained.

Furthermore, on a series of Fe_xC_y surfaces, surface C hydrogenation to CH_4 exhibits different thermodynamic and kinetic characteristics. On $Fe_2C(011)$, $Fe_5C_2(010)$, $Fe_3C(001)$, and $Fe_4C(100)$, the most stable C_1 species are C/CH_3, CH/CH_2, CH, and C, respectively. According to the calculated reaction

(35) For confirming this linear relationship, several less stable surfaces with different structures (Figure S1), $Fe_2C(001)$, $Fe_5C_2(001)$, $Fe_3C(100)$, and $Fe_4C(111)$, are also examined thermodynamically. As expected, not only the most stable surfaces but also the less stable surfaces fit the line very well.

(36) van Santen, R. A.; Neurock, M. *Molecular Heterogeneous Catalysis*; Wiley−VCH: Weinheim, 2006.

(37) Pallassana, V.; Neurock, M. *J. Catal.* **2000**, *191*, 301.

(38) Ciobica, I. M.; van Santen, R. A. *J. Phys. Chem. B* **2002**, *106*, 6200.

(39) Lo, J. M. H.; Ziegler, T. *J. Phys. Chem. C* **2007**, *111*, 11012.

energies and effective barriers, CH_4 formation is more favorable on $Fe_5C_2(010)$ (−0.23 and 1.54 eV) and $Fe_2C(011)$ (−0.14 and 1.36 eV), while $Fe_4C(100)$ (0.30 and 1.94 eV) and $Fe_3C(001)$ (−0.18 and 1.98 eV) are inactive toward CH_4 formation.

More importantly, it is revealed that reaction energy ($\Delta_r E$) and effective barrier (E_{eff}) for CH_4 formation exhibit a linear relationship with the charge of the surface C atom and the d-band center (ε_d) of the surface, respectively. This finding can help us understand the reactivity of all active surfaces via analyzing their surface properties and further guiding the catalyst design in FTS.

Acknowledgment. We would like to thank Prof. Peijun Hu (The Queen's University of Belfast) for helpful discussions. The National Natural Science Foundation of China (No. 20873173), the National Outstanding Young Scientists Foundation of China (No. 20625620), and Synfuels CHINA are acknowledged for financial support.

Supporting Information Available: Total energies and key bond parameters (Tables S1−S4) as well as Cartesian coordinates for all stationary points. This material is available free of charge via the Internet at http://pubs.acs.org.

JA9021864